metals

MDPI

Article

The Mechanism of Oxide Growth on Pure Aluminum in Ultra-High-Temperature Steam

Lin Huang [1,2], Ke Xiong [1,2], Xiaofeng Wang [1,2], Xi He [1,2], Lin Yu [1,3], Chaokun Fu [2,4], Xiaodong Zhu [1,2,*] and Wei Feng [1,2,*]

[1] School of Mechanical Engineering, Chengdu University, Chengdu 610106, China; huanglin@cdu.edu.cn (L.H.); 13281467267@163.com (K.X.); 13880073327@163.com (X.W.); h2404522805@163.com (X.H.); 13658066449@163.com (L.Y.)
[2] Sichuan Powder Metallurgy Engineering Technology Research Center, Chengdu 610106, China; kuntian@vip.163.com
[3] Sichuan Yiran Material Technology Co., Ltd., Chengdu 610100, China
[4] Sichuan KunTian Cemented Carbide Co., Ltd., Yibin 644001, China
* Correspondence: zhuxiaodong@cdu.edu.cn (X.Z.); fengwei@cdu.edu.cn (W.F.)

Abstract: A high-temperature water steam ($H_2O(g)$) between 300 °C and 1000 °C reacted with the Al surface in this study. The Al surface states were characterized and analyzed using XRD °C, XPS, and SEM after and before the reaction, and the effects and mechanism of $H_2O(g)$ on the Al surface morphology and chemical composition were studied. The experiment showed that for an Al sheet reacting with $H_2O(g)$, its oxide layer morphology changed from nano-needle to flaky and granular oxides gradually with the rise of temperature, and finally the Al surface became porous as a whole. Its oxide crystals were amorphous and were determined to be aluminum oxide (Al_2O_3) using XPS. The needle-like oxide in the Al sheet surface tended to grow toward the surface, and no obviously inward oxidizing corrosion layer occurred in the aluminum substrate; the oxide layer between the oxide and Al sheet substrate was compact, and could effectively prevent the infiltration and corrosion of water molecules.

Keywords: Al; high temperature water steam; corrosion; surface states; oxide layer

Citation: Huang, L.; Xiong, K.; Wang, X.; He, X.; Yu, L.; Fu, C.; Zhu, X.; Feng, W. The Mechanism of Oxide Growth on Pure Aluminum in Ultra-High-Temperature Steam. *Metals* **2022**, *12*, 1049. https://doi.org/10.3390/met12061049

Academic Editor: Frank Czerwinski

Received: 9 May 2022
Accepted: 16 June 2022
Published: 19 June 2022

1. Introduction

Pure aluminum has a greater affinity with oxygen and can be automatically oxidized in atmospheric environments to form an Al_2O_3 passivation film that is 0.005 to 0.015 μm thick. The film is very compact, and can effectively prevent further aluminum oxidation; it can remain stable even at fairly high temperatures [1]. A comparative study on the antioxidant properties of the heat-resistant Fe−Cr alloy and Fe−Cr−Ni−Al alloy [2–8] found that the aluminum oxide film in the Fe−Cr−Ni−Al alloy was more stable than the chromium oxide film [9]. Therefore, the aluminum oxide film that formed in the air did not only have a better wear resistance to atmospheric corrosion, but it could also help improve the anti-atmosphere oxidation performance of alloy materials when the aluminum was added in the form of alloy elements [10–14]. However, in the actual engineering application of aluminum, in addition to seawater, atmosphere, salt fog, and other environmental factors, there is also high-temperature air and water vapor corrosion, which often forms a variety of aluminum amorphous hydrate, and its hardness is not high, its wear resistance is poor, and thus it has a negative impact on the engineering application of aluminum [15–17]. J.M. Guilemany et al. studied the oxidation behavior of Fe40Al coating in the air at 900 °C, 1000 °C, and 1100 °C. Compared with the matrix, the existence of Al leads to more significant corrosion resistance of the coating, and the oxidation layer is uniform and continuous at 900 °C, and stable α-Al_2O_3 is not detected at high temperatures of 1000 °C and 1100 °C; based on the results of this study, it is speculated that 900 °C may

be the boundary temperature of the oxidation resistance of the coating [18]. However, the corrosion of aluminum under high-temperature water vapor conditions (300~1000 °C) has not been reported. Based on the aluminum material and high aluminum refractory steel containing aluminum alloy materials such as those possible under an environment of high-temperature steam engineering applications [19], this paper uses its own patent research to develop a superheated vapor reaction device [20]. The behavior of the water vapor and the physical and chemical properties of aluminum in a high temperature environment of 300~1000 °C are studied in order to provide theoretical support for the practical engineering application of aluminum and its alloys.

2. Materials and Methods

2.1. Experimental Materials and Process

An aluminum sheet with a purity of 99.99% and a thickness of 0.1 mm (General Research Institute for Nonferrous Metals, Beijing, China) was employed as the experimental material. The aluminum sheet was first cut to a 12 × 12 mm size, and was then polished and rinsed ultrasonically three times using waterless ethanol, acetone, and secondary deionized water, separately. The pure reagents were used for the analysis in the experiment. During the experiment, the temperature fluctuation was controlled within ±0.3 °C, the gas filling rate was at 10 to 15 mL/s, and the reaction time was 5 min. A self-built high temperature water vapor reaction device was used as the test reactor, as shown in Figure 1. The aluminum sheets were dried and placed into the Φ20 quartz tube, as shown in Figure 1; the Ar gas was filled from the gas inlet of the quartz tube to drain the air. The secondary deionized water was heated to the experimental temperature using the quartz steam generator, and the pipe heater and the water vapor flow meter were adjusted to allow high-temperature water vapor ($H_2O(g)$) to flow into the quartz tube. After the water vapor was heated using the heating device and it reacted with the sample, it was freely discharged from the exhaust port of the quartz tube furnace, and the pressure in the tube was maintained at a constant atmospheric pressure. The quartz tube furnace was heated to the experimental set temperature, then the quartz tube with aluminum sheets was placed into the furnace for the reaction of the aluminum sheets with $H_2O(g)$; the Ar gas was gradually turned off. After reaching the set experimental reaction time, the Ar gas was filled in and the $H_2O(g)$ was closed off gradually, and the quartz tube was taken out and cooled to room temperature; finally, the Ar gas was cut off and the aluminum sheets were taken out of the quartz tube.

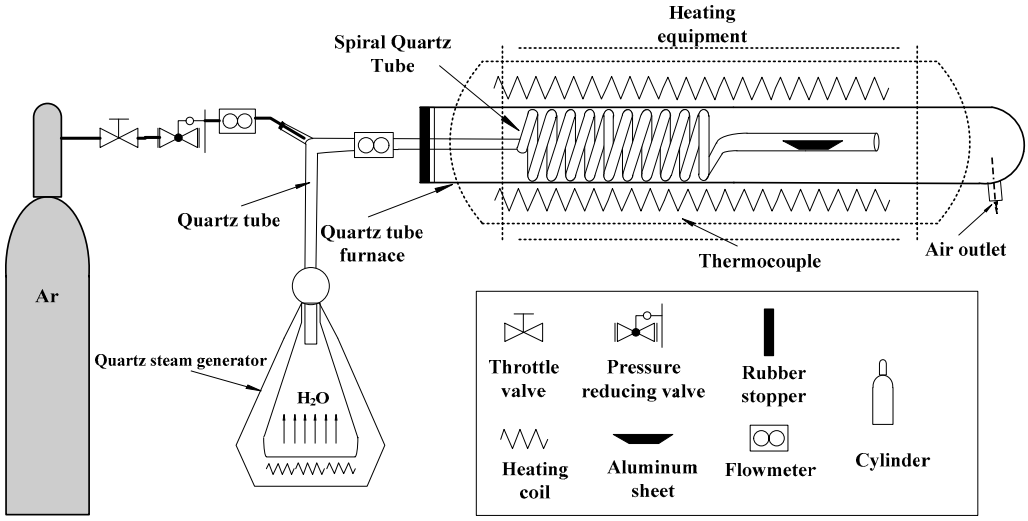

Figure 1. System drawing of the experiment [20].

2.2. Analysis and Characterization

The sample phase analysis was carried out using the DX-2500 X-ray diffraction machine (XRD, Dandong Haoyuan Instrument Co. Ltd., Dandong, China). The test conditions were as follows: Cu target Kα ray, tube voltage of 40 kV, tube current of 40 mA, scanning angle range of 30~70°, step angle of 5°/min, and sampling time of 1 s. The surface micro-morphology was determined using the Quanta 450 FEG field emission scanning electron microscope (FEI Company, Hillsboro, OR, USA), and the surface chemical state was analyzed using an ESCALAB Model 250 X-ray photoelectronic energy spectrometer (XPS, Thermo Scientific K-Alpha, Kratos Ltd., Manchester, UK).

3. Results and Discussion

3.1. Effects of High-Temperature Water Vapor on the Aluminum Surface Chemical State

Figure 2 shows the XRD test results of the aluminum surface under different reaction conditions. It can be seen from the figure that after the reaction of the aluminum sheet with water vapor at 300 °C to 1000 °C, its diffraction peaks were consistent with the XRD characteristic peaks of elemental Al, and no characteristic peaks for the oxide phase were detected. In order to further understand the oxidation of the aluminum surface, XPS was used to analyze the aluminum surface. Figure 3a provides the results regarding the survey-spectrum chemical elements tested using XPS on the surface of the aluminum sheets after their reaction with the aluminum surface at 400 °C. It can be seen that the O 1s, C 1s, and Al 2p were observed on survey spectrum, and O 1s is very bright at 531.3 eV BE in Figure 3c, indicating that the oxygen content is high on the surface of the Al sheet. More details on the high-resolution spectrum of Al 2p at a binding energy of 74.3 eV is a characteristic peak of Al^{3+}, as shown in Figure 3b, providing evidence that the surfaces of the Al sheets were oxidized, which is consistent with the literature [21]. The peaks at 531.3 eV BE and 74.3 eV BE were derived from the deconvolution of the high-resolution single peak of O 1s and Al 2p, respectively. As Al_2O_3 can also appear on the aluminum surface in the atmosphere and can form a dense oxide layer to prevent further oxidation of the matrix, the XPS test results show that Al_2O_3 is indeed present on the aluminum surface, but the XRD test could not detect the presence of the Al_2O_3 phase, which just shows that the thickness of the oxide layer after reacting with high-temperature water vapor is very thin, which is similar to the thickness of the oxide film formed on the surface of the aluminum after oxidation in air at room temperature, and its thickness does not increase significantly at high temperatures. At high temperatures, the reaction process between the aluminum surface and water vapor should be as follows:

$$2Al + 6H_2O_{(g)} \xrightarrow{\Delta} 2Al + 12H^+ + 6O^{2-} \xrightarrow{\Delta} Al_2O_3 + 3H_2O^{\uparrow}{}_{(g)} + 3H_2{}^{\uparrow} \quad (1)$$

Based on this contradictory situation in the XRD testing and XPS analysis, this is possibly caused by too little peak strength from the too low crystallization, because the resulting oxide crystals are nearly amorphous [22]. This can also reveal that aluminum in high temperature water vapor will produce a thin oxide layer at a lower temperature, and this oxide layer grows less obviously with the rise of temperature. This layer of oxide film is compact to prevent further oxidation of the aluminum surface, so that the aluminum has a good stability and resistance to water vapor corrosion [23].

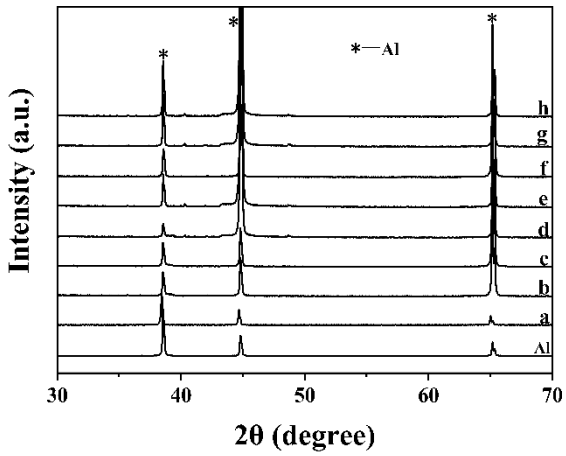

Figure 2. XRD spectrograms of the aluminum sheet surface: (**a**) after reaction with 300 °C of H_2O(g); (**b**) after reaction with 400 °C of H_2O(g); (**c**) after reaction with 500 °C of H_2O(g); (**d**) after reaction with 600 °C of H_2O(g); (**e**) after reaction with 700 °C of H_2O(g); (**f**) after reaction with 800 °C of H_2O(g); (**g**) after reaction with 900 °C of H_2O(g); (**h**) after reaction with 1000 °C of H_2O(g).

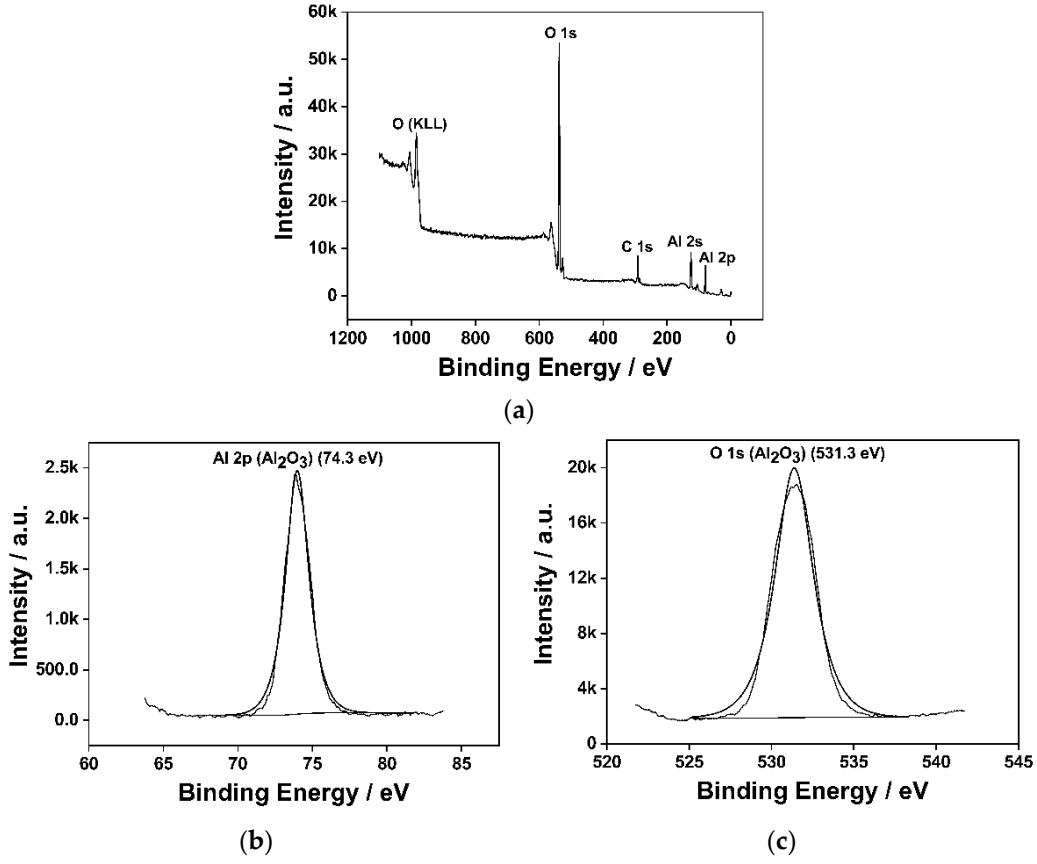

Figure 3. XPS spectrograms of the aluminum surface after reaction with 400 °C of water vapor: (**a**) survey spectrum of the sample surface elements; (**b**) the high-resolution single peak of Al 2p; (**c**) the high-resolution single peak of O 1s.

3.2. Effects of High Temperature Water Vapor on the Aluminum Surface Morphology

There are no significant changes in the phase information obtained from the XRD test, indicating that the aluminum sheet surface has not yet produced enough thick enough oxides to be detected by XRD. For this reason, it is unlikely that the aluminum sheet surface has significant changes in morphology. However, because of the production

of significant oxides found in XPS detection, the possibility of changes in the surface microstructure remains. Because the oxide layer formed on its surface hinders further oxidation of the aluminum surface, the thickness of its oxide film does not change obviously with temperature [24]. Therefore, its surface morphology should change mostly in the structure and the resulting shape. Figure 4 shows the surface morphology of the aluminum sheet after reacting with water vapor at different temperatures, revealing the formation of oxide products on the aluminum surface at the same temperature holding time. As can be seen from Figure 4a–e, the aluminum sheet surface became noticeably rough from 300 to 700 °C, resulting in a needle-like product of about 10 nm in diameter and 60–80 nm in length. In Figure 4f, as the temperature rises to 800 °C, the needle-like product becomes significantly thick, with 20–30 nm in diameter, but it does not change much in length. As the temperature rises further, the single needle-like product grows less noticeably in volume, but there is a tendency that these needle-like products will come into contact with each other and bind into the granular products. When the temperature reaches 900 °C, the needle-like product gradually changes to the flaky one in Figure 4g. When the temperature reaches 1000 °C, as shown in Figure 4h, the flake-like products are further combined to form a granular structure.

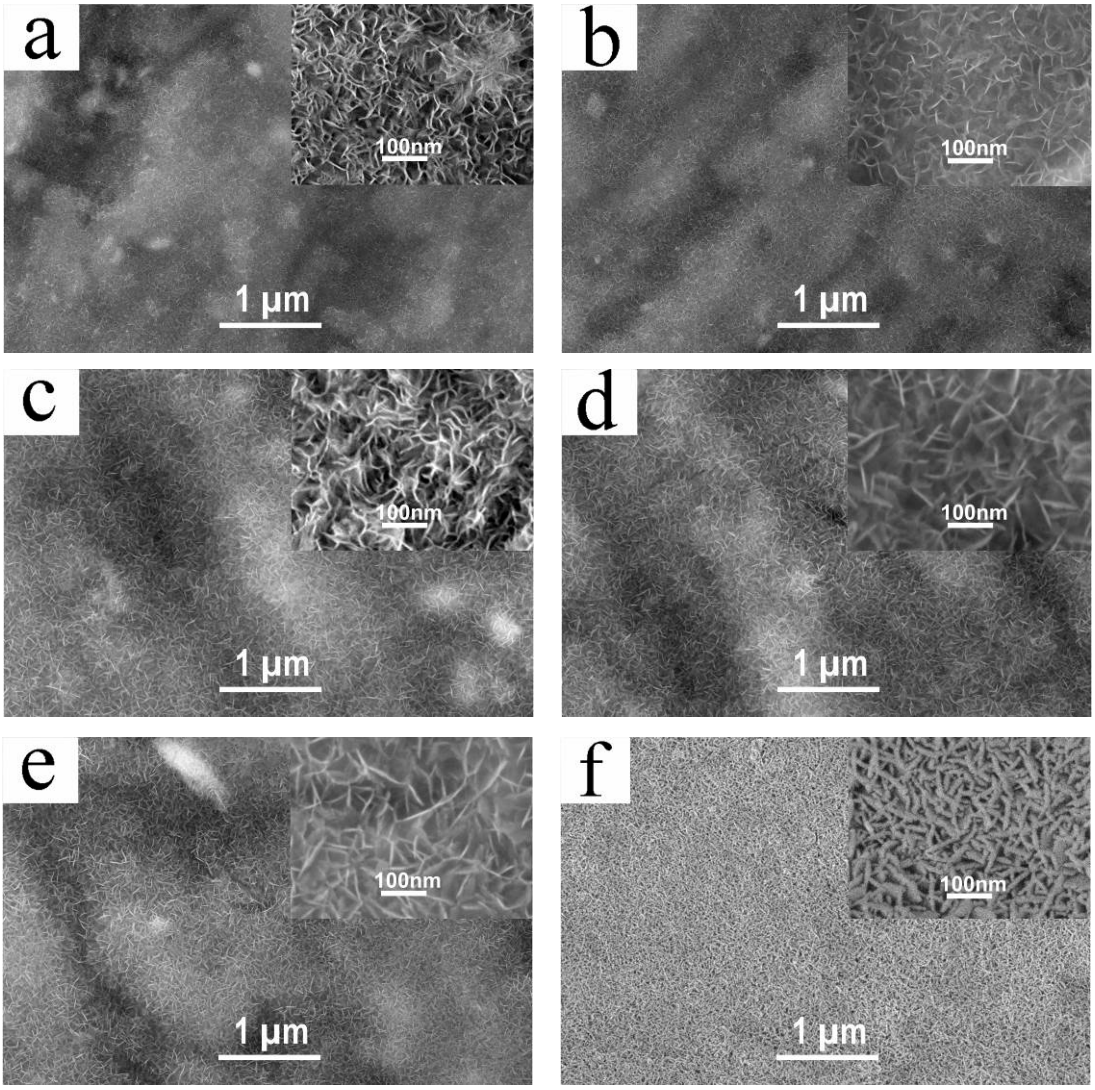

Figure 4. *Cont.*

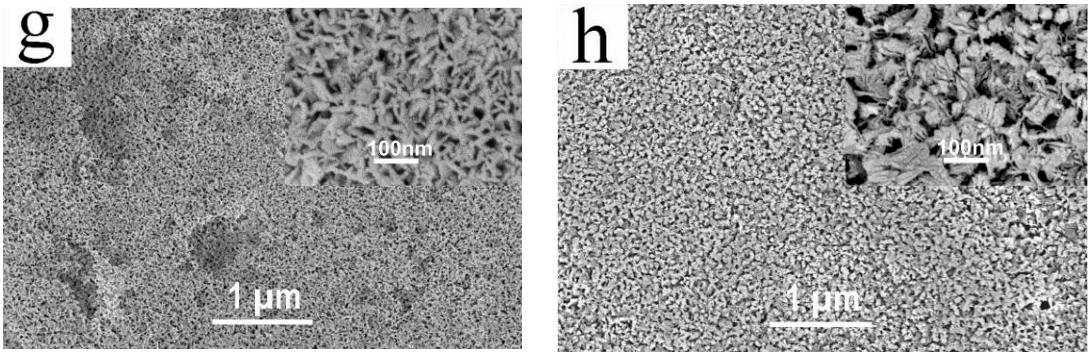

Figure 4. Surface morphology of the aluminum sheets after reacting with water vapor at different temperatures: (**a**) 300 °C; (**b**) 400 °C; (**c**) 500 °C; (**d**) 600 °C; (**e**) 700 °C; (**f**) 800 °C; (**g**) 900 °C; (**h**) 1000 °C.

In the gas–solid reaction, the migration of substances is relatively difficult, especially in the case of a relatively short time. With the increase in the reaction temperature, the number of crystal nucleation increases, and the speed of crystal growth is relatively slow, so this may be the main factor in the appearance of this shape. After the XRD test, no Al_2O_3 phase is found on the aluminum surface, so XPS can be used to detect the presence of Al_2O_3 oxide at a lower reaction temperature (400 °C), and the resulting oxide layer can be very thin. As the temperature continues to increase, the results of the XPS test should also be the same, so there is no need for further XPS testing.

3.3. The Corrosive Layer Structure of an Aluminum Sheet Corroded by High Temperature Water Vapor

In order to further understand the influence of high temperature water vapor on the corrosion of aluminum sheets, the experiment of an aluminum sheet after high-temperature water vapor reaction at 700 °C, a common engineering temperature, was selected for analysis [25]. From the overall structure of the aluminum sheet, Figure 5 shows a sectional diagram of the aluminum sheet corroded by high-temperature water vapor at 700 °C. From the point of view of the junction between the oxide layer and the substrate, Figure 5a shows that no obvious oxide layering occurs in the section of aluminum sheet, and Figure 5b reveals that there is a very thin layer of needle-like oxide product on the aluminum sheet surface; in the slight plastic deformation when the aluminum sheet is cut, the oxide product is stretched and separated, but no oxide is stripped off or cracked from the Al sheet substrate. The acicular oxide is tightly combined with the aluminum substrate, and there is no obvious delamination phenomenon. From below the oxide surface layer, in Figure 5c, it is seen that the needle-like oxide is closely combined with the aluminum sheet substrate, and no obvious layering occurs. The material below the needle oxide is compact, and there is no infiltration of the oxide into the interior. The compact oxidizing layer generated between the needle-like oxide and the aluminum sheet substrate effectively prevents the corrosion of the aluminum sheet by water vapor. The reason for the change of oxide morphology is the fusion and growing of oxide grains [26].

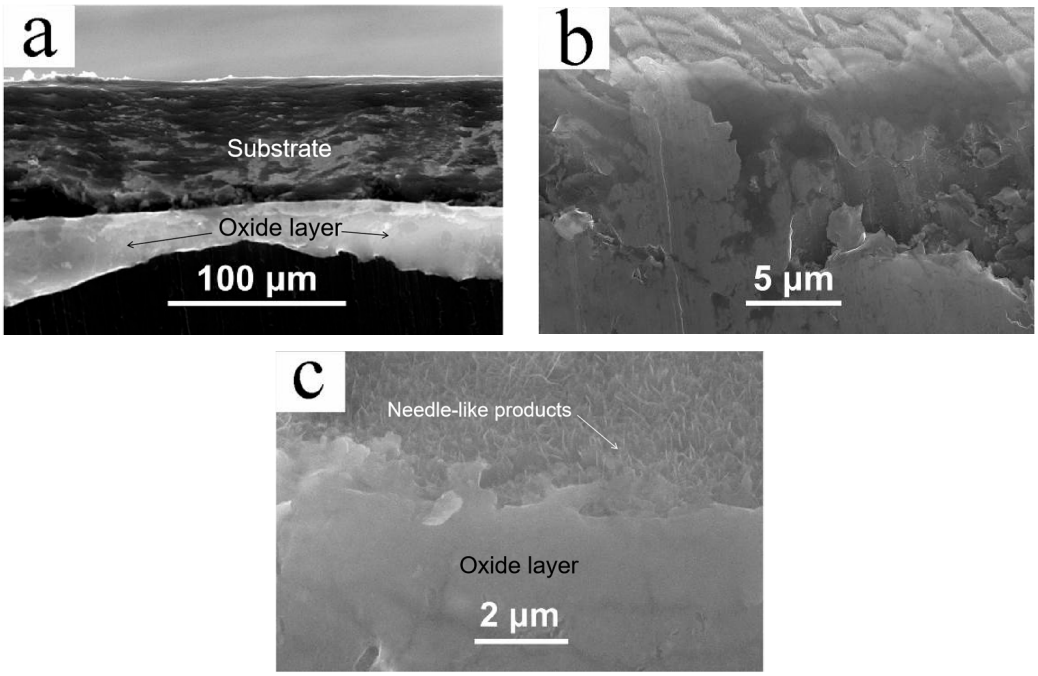

Figure 5. Cross-sectional view of an aluminum sheet corroded under high-temperature water vapor at 700 °C: (**a**) Aluminum sheet overall structure; (**b**) Bonding site of oxide layer and substrate; (**c**) Below the oxide surface layer.

4. Conclusions

1. The oxide phase cannot be detected by XRD for an aluminum sheet after 5 min of reaction with high temperature water vapor, indicating that the oxide crystals are nearly amorphous with too low crystallization, resulting in a too small peak strength. The chemical state of the oxide can be detected very well by XPS, and the oxidation product can be determined as Al_2O_3.
2. The needle-like nano-oxidation product is produced at 300 °C on the Al sheet surface after the reaction of the aluminum sheet with high temperature water vapor. The needle-like nano-oxidation gradually is gradually thickened with the temperature rising. Combined with adjacent needle-like oxides after contact, it gradually forms flaky and granular oxide products, so that the aluminum surface presents a porous state as a whole.
3. The section analysis reveals that no significant inward oxidizing corrosion layer occurs in the aluminum substrate below the needle-like oxide on the aluminum sheet surface, indicating that the compact oxide layer forms between the needle-like oxide and the aluminum sheet substrate, and it can effectively prevent the infiltration and corrosion of water molecules.

Author Contributions: Conceptualization, W.F. and X.Z.; methodology, K.X. and L.H.; validation, K.X., X.W., and X.H.; formal analysis, L.H., K.X., and X.W.; investigation, K.X., X.H., and L.Y.; resources, L.H., C.F. and X.Z.; data curation, L.H. and K.X.; writing—original draft preparation, K.X. and L.H.; writing—review and editing, L.H., K.X., and X.Z.; visualization, W.F.; supervision, W.F. and X.Z.; project administration, W.F.; funding acquisition, L.H. All authors have read and agreed to the published version of the manuscript.

Funding: This research was supported by the Sichuan Province Application Fundamental Key Project (grant no. 2018JY0062) and the National Major Special Project Sub-project (grant no. 2015GB1110002B-3).

Institutional Review Board Statement: Not applicable.

Informed Consent Statement: Not applicable.

Data Availability Statement: Data are contained within the article.

Conflicts of Interest: The authors declare no conflict of interest.

References

1. Nalivaiko, A.Y.; Arnautov, A.N.; Zmanovsky, S.V.; Ozherelkov, D.Y.; Gromov, A.A. Al–Al_2O_3 powder composites obtained by hydrothermal oxidation method: Powders and sintered samples characterization. *J. Alloys Compd.* **2020**, *825*, 154024. [CrossRef]
2. Liu, X.G.; Mao, Q.S.; Jiang, Y.; Li, Y.; Sun, J.L.; Huang, F.X. Preparation of Al_2O_3–SiO_2 composite aerogels and their cu2+absorption properties. *Int. J. Miner. Metall. Mater.* **2021**, *28*, 317–324. [CrossRef]
3. Tishkevich, D.I.; Vorobjova, A.I.; Trukhanov, A.V. Thermal stability of nano-crystalline nickel electrodeposited into porous alumina. *Solid State Phenom.* **2020**, *299*, 281–286. [CrossRef]
4. Saa, B.; Iac, D.; Za, A.; Aj, E.; Mna, F.; As, A. Fabrication and corrosion inhibition behavior of hierarchical Al-Cr Co-doped magnesium ferrites nanomaterial for steel. *Surf. Coat. Technol.* **2021**, *405*, 126687.
5. Yaokawa, J.; Oh-Ishi, K.; Dong, S. Estimation of dimensional change of Al–10Si–Mg alloy castings during heat treatment. *Mater. Trans.* **2021**, *62*, 1023–1029. [CrossRef]
6. Sadatoshi; Koroyasu. Effects of reduced pressure, casting design and heat transfer resistance of liquid resin on mold filling in expendable pattern casting process of aluminum alloy. *Mater. Trans.* **2020**, *61*, 528–533. [CrossRef]
7. Xing, L.; Zheng, Y.; Cui, L.; Sun, M.; Shao, M.; Lu, G. Formation of alumina layer on fe-cr-ni alloy by pack cementation and oxidation. *High Temp. Mater. Processes* **2011**, *30*, 99–103. [CrossRef]
8. Muhammad, R.; Motohiro, Y.; Hiroyuki, M. Enhanced corrosion resistance of ultrafine-grained Fe-Cr alloys with subcritical cr contents for passivity. *Metals* **2018**, *8*, 149.
9. Qiao, L.; Bao, A.; Wang, Y.; Liu, Y.; Zhu, J. Thermophysical properties and high temperature oxidation behavior of fecrnial 0.5 multi-component alloys. *Intermetallics* **2020**, *126*, 106899. [CrossRef]
10. Stallybrass, C.; Schneider, A.; Sauthoff, G. The strengthening effect of (Ni,Fe)Al precipitates on the mechanical properties at high temperatures of ferritic Fe–Al–Ni–Cr alloys. *Intermetallics* **2005**, *13*, 1263–1268. [CrossRef]
11. Pei-Qing, L.A.; Li, Z.; Liu, Z.Y.; Wang, W.G.; Yan, F.Y.; Yuan, H. Effect of aluminum on microstructure of hp40 alloy. *J. Iron Steel Res. Int.* **2008**, *14*, 373–377.
12. Shao, L.; Shi, Y.; Huang, J.K.; Wu, S.J. Effect of joining parameters on microstructure of dissimilar metal joints between aluminum and galvanized steel. *Mater. Des.* **2015**, *66*, 453–458. [CrossRef]
13. Peng, S.; Tian, D.; Miao, X.; Yang, X.; Deng, W. Designing robust alumina nanowires-on-nanopores structures: Superhydrophobic surfaces with slippery or sticky water adhesion. *J. Colloid Interface Sci.* **2013**, *409*, 18–24. [CrossRef] [PubMed]
14. Lee, M.H.; Lim, N.; Ruebusch, D.J.; Jamshidi, A.; Kapadia, R.; Lee, R.; Seok, T.J.; Takei, K.; Cho, K.Y.; Fan, Z. Roll-to-roll anodization and etching of aluminum foils for high-throughput surface nanotexturing. *Nano Lett.* **2011**, *11*, 3425–3430. [CrossRef] [PubMed]
15. Rambabu, G.; Naik, D.B.; Rao, C.; Rao, K.S.; Reddy, G.M. Optimization of friction stir welding parameters for improved corrosion resistance of aa2219 aluminum alloy joints. *Def. Technol.* **2015**, *11*, 330–337. [CrossRef]
16. Xue, H.W.; Cheng, Y.L.; Chen, G.; He, L.; Cao, H. Preparation and thermal stability of porous alumina membranes with nano-pore arrays. *Appl. Phys. A Mater. Sci. Processing* **2010**, *98*, 745–749.
17. Syed, R.; Sen, D.; Krishna, K.V.M.; Ghosh, S. Fabrication of highly ordered nanoporous alumina membranes: Probing microstructures by saxs, fesem and afm. *Microporous Mesoporous Mater.* **2018**, *264*, 13–21. [CrossRef]
18. Yilbas, B.S.; Arif, A.F.M.; Karatas, C. Laser treatment of silicon at nitrogen ambient: Thermal stress analysis. *Surf. Eng.* **2011**, *27*, 436–444. [CrossRef]
19. Guilemany, J.M.; Cinca, N.; Dosta, S.; Lima, C. High-temperature oxidation of fe40al coatings obtained by hvof thermal spray. *Intermetallics* **2007**, *15*, 1384–1394. [CrossRef]
20. Feng, W.; Wang, Q.; Kong, Q.; Zhu, X.; Wu, J.; Sun, C. Influence of high-temperature water vapor on titanium film surface. *Oxid. Met.* **2016**, *86*, 179–192. [CrossRef]
21. Leinen, D.; Lassaletta, G.; Fernandez, A.; Caballero, A.; Gonzalez-Elipe, A.R.; Martin, J.M.; Vacher, B. Ion beam induced chemical vapor deposition procedure for the preparation of oxide thin films. Ii. Preparation and characterization of alxtiyoz thin films. *J. Vac. Sci. Technol. A Vac. Surf. Film.* **1996**, *14*, 2842–2848. [CrossRef]
22. Kathirvel, P.; Chandrasekaran, J.; Manoharan, D.; Kumar, S. Preparation and characterization of alpha alumina nanoparticles by in-flight oxidation of flame synthesis. *J. Alloy. Compd.* **2013**, *590*, 341–345. [CrossRef]
23. Oja, M.; Feldbach, E.; Kirm, M. Relaxation of intrinsic and extrinsic electronic excitations in nano- and micro-size alumina. *Opt. Mater.* **2019**, *91*, 120–125. [CrossRef]
24. Zhou, D.Q.; Zhao, W.X.; Mao, H.H.; Hu, Y.X.; Xu, X.Q.; Sun, X.Y.; Lu, Z.P. Precipitate characteristics and their effects on the high-temperature creep resistance of alumina-forming austenitic stainless steels. *Mater. Sci. Eng. A.* **2015**, *622*, 91–100. [CrossRef]
25. Zheng, Q.; Wu, J.; Jiang, H.; Zhang, L.; Zhao, J.; He, J. Effect of micro-alloying element la on corrosion behavior of Al-Mg-Si alloys. *Corros. Sci.* **2021**, *179*, 109–113. [CrossRef]
26. Wang, J.; Liu, S.; Bai, X.; Zhou, X.; Han, X. Oxidation behavior of fe-al-cr alloy at high temperature: Experiment and a first principle study. *Vacuum* **2019**, *173*, 109144. [CrossRef]